LITHOS

New insights on the porosity and grain features of Al Haggounia 001, an impact-melt meteorite

--Manuscript Draft--

Manuscript Number:	LITHOS10904
Article Type:	Regular Article
Keywords:	EL3 impact melt meteorite 1; pores and vesicles 2; sulfides 3
Corresponding Author:	Giovanna Agrosì, Ph.D. University BARI, Bari ITALY
First Author:	Paola Manzari, Ph.D. researcher
Order of Authors:	Paola Manzari, Ph.D. researcher
	Daniela Mele, Ph.D. professor
	Gioacchino Tempesta, Ph.D. professor
	Giovanna Agrosì, Ph.D. professor
Abstract:	In the frame of a broader study on impact effects on meteorites microstructures and mineralogy, we studied the internal structures and grain features of Al Haggounia 001 meteorite, a very interesting EL3 impact melt characterized by a strong porosity. The study was carried out using a 3D reconstruction obtained by micro-Computed x-ray Tomography (μ-CT) supported by chemo-mineralogical characterization obtained by SEM-EDS. The fragments examined consist of a matrix of enstatite, plagioclase, with minor phases such as sulfides, oxides, and phosphides. Only one relict chondrule was observed that consists of a radial pyroxene with enstatite composition, Na plagioclase and silica mesostasis. SEM-EDS analyses reveal that the average composition of pyroxene and plagioclase is (En 98.4 Fs 0 Wo 1.6) and (Ab 80 An 12 Or 8), respectively. The minor phases found are daubréelite, schreibersite, oldhamite, troilite, graphite, tiny kamacite grains survived to the weathering, and N-bearing oxide. In addition to primary phases, terrestrial products as jarosite and halite were found. Kamacite appears variably oxidized. HR-SEM images reveal resorption features as well as rounded etch pits on the surfaces of daubréelite, holes on plagioclase and scalloped enstatite crystals. The μ-CT measurements show an uneven porosity with an average percentage of about 15% that consists averagely of open pores (12%) and closed pores (3%) with irregular to round shapes. The innovative methodological approach, based on volumetric investigation, providing information about the spatial distribution, volume percentage and shape of voids and mineralogical phases with different density, add new elements about the origin of porosity in this meteorite.
Suggested Reviewers:	Costanza Bonadiman, PhD Professor, University of Ferrara costanza.bonadiman@unife.it She is an expert of meteorites
	Mara Murri, PhD researcher, University of Milan-Bicocca mara.murri@unimib.it she is an expert of meteorites
	Matteo Alvaro, PhD Professor, University of Pavia matteo.alvaro@unipv.it he is an expert of meteorites
	Davide Novella, PhD researcher, University of Padua davide.novella@unipd.it he is an expert of global geochemical cycles and magmatic processes
	Isabella Pignatelli, PhD

	assistant professor, UL University isabella.pignatelli@univ-lorraine.fr expert of meteorites and micro-CT analyses
	Hasnaa Chennaoui Aoudjehane, PhD professor, University Hassan II Casablanca hassna.chennaoui@univh2c.ma expert of meteorites
Opposed Reviewers:	

New insights on the porosity and grain features of Al Haggounia 001, an impact-melt meteorite

Paola Manzari [1], Daniela Mele[2], Gioacchino Tempesta[2] and Giovanna Agrosì [2*]

[1] Italian Space Agency, Rome, Italy
[2] Department of Earth and Geo-environmental, University of Bari "Aldo Moro", Bari, Italy
* Corresponding author: Giovanna Agrosì giovanna.agrosi@uniba.it

Cover letter ***Bari, August 13, 2022***

Dear Editor,

we wish to submit the manuscript entitled: “New insights on the porosity and grain features of Al Haggounia 001, an impact-melt meteorite” by Paola Manzari, Daniela Mele, Gioacchino Tempesta and Giovanna Agrosì, for your consideration for publication on LITHOS.

The manuscript presents a novel approach based on three dimensionally reconstruction of a volume of slab of Al Haggounia 001 meteorite, in which the spatial distribution of mineralogical phases and voids, their volume percentage, shape, and size were studied.

The study was carried out on a fragment of meteorite (thin section and slab) combining a 3D reconstruction of pores and grain features, obtained by micro-Computed x-ray Tomography (µ-CT), with chemo-mineralogical characterization obtained of phases by SEM-EDS.

The volumetric analyses used in this work providing information about the spatial relationships between open and closed pores and mineralogical phases, add new evidence about the origin of porosity in Al Haggounia 001 meteorite, distinguishing a primary porosity related to degassing of sulfides during impact melting event from a secondary porosity caused by terrestrial weathering.

On behalf of my co-authors

Best regards

Giovanna Agrosì

Dipartimento di Scienze della Terra e Geoambientali

Università di Bari

Via E. Orabona 4, 70125

Phone: +393395367006

Email: giovanna.agrosi@uniba.it

Bari, Italy

In the frame of a broader study on impact effects on meteorites microstructures and mineralogy, we studied the internal structures and grain features of Al Haggounia 001 meteorite, a very interesting EL3 impact melt characterized by a strong porosity. The study was carried out using a 3D reconstruction obtained by micro-Computed x-ray Tomography (µ-CT) supported by chemo-mineralogical characterization obtained by SEM-EDS. The fragments examined consist of a matrix of enstatite, plagioclase, with minor phases such as sulfides, oxides, and phosphides. Only one relict chondrule was observed that consists of a radial pyroxene with enstatite composition, Na plagioclase and silica mesostasis. SEM-EDS analyses reveal that the average composition of pyroxene and plagioclase is ($En_{98.4}$ Fs_{0} $Wo_{1.6}$) and (Ab_{80} An_{12} Or_{8}), respectively. The minor phases found are daubréelite, schreibersite, oldhamite, troilite, graphite, tiny kamacite grains survived to the weathering, and N-bearing oxide. In addition to primary phases, terrestrial products as jarosite and halite were found. Kamacite appears variably oxidized. HR-SEM images reveal resorption features as well as rounded etch pits on the surfaces of daubréelite, holes on plagioclase and scalloped enstatite crystals. The µ-CT measurements show an uneven porosity with an average percentage of about 15% that consists averagely of open pores (12 %) and closed pores (3%) with irregular to round shapes. The innovative methodological approach, based on volumetric investigation, providing information about the spatial distribution, volume percentage and shape of voids and mineralogical phases with different density, add new elements about the origin of porosity in this meteorite.

- volumetric analyses of porosity and grain features of Al-Haggounia 001 meteorite
- combined use of μ-CT and microanalyses to reconstruct the 3D internal structure
- total porosity consists of open and closed pores with different genetic implications
- links among spatial distribution, vol% and sizes of pores and mineralogical phases

New insights on the porosity and grain features of Al Haggounia 001, an impact-melt meteorite

Paola Manzari [1], Daniela Mele[2], Gioacchino Tempesta[2] and Giovanna Agrosì [2*]

[1] Italian Space Agency, Rome, Italy
[2] Department of Earth and Geo-environmental, University of Bari "Aldo Moro", Bari, Italy
* Corresponding author: Giovanna Agrosì giovanna.agrosi@uniba.it

Abstract:

In the frame of a broader study on impact effects on meteorites microstructures and mineralogy, we studied the internal structures and grain features of Al Haggounia 001 meteorite, a very interesting EL3 impact melt characterized by a strong porosity. The study was carried out using a 3D reconstruction obtained by micro-Computed x-ray Tomography (μ-CT) supported by chemo-mineralogical characterization obtained by SEM-EDS. The fragments examined consist of a matrix of enstatite, plagioclase, with minor phases such as sulfides, oxides, and phosphides. Only one relict chondrule was observed that consists of a radial pyroxene with enstatite composition, Na plagioclase and silica mesostasis. SEM-EDS analyses reveal that the average composition of pyroxene and plagioclase is ($En_{98.4}$ Fs_{0} $Wo_{1.6}$) and (Ab_{80} An_{12} Or_{8}), respectively. The minor phases found are daubréelite, schreibersite, oldhamite, troilite, graphite, tiny kamacite grains survived to the weathering, and N-bearing oxide. In addition to primary phases, terrestrial products as jarosite and halite were found. Kamacite appears variably oxidized. HR-SEM images reveal resorption features as well as rounded etch pits on the surfaces of daubréelite, holes on plagioclase and scalloped enstatite crystals. The μ-CT measurements show an uneven porosity with an average percentage of about 15% that consists averagely of open pores (12 %) and closed pores (3%) with irregular to round shapes. The innovative methodological approach, based on volumetric investigation, providing information about the spatial distribution, volume percentage and shape of voids and mineralogical phases with different density, add new elements about the origin of porosity in this meteorite.

Keywords: EL3 impact melt meteorite 1; pores and vesicles 2; sulfides 3

1. Introduction

The "fossil meteorite" [1 (Bunch et al., 2014)], Al Haggounia 001, is a EL3 impact melt rock (Rubin 2016). It is an interesting meteorite because, with paired samples named Northwest Africa (NWA), with a total mass of about 3 tons (MBD), represent the largest enstatite meteorite known. This meteorite was found in 2006 in western Sahara in sedimentary rocks such as conglomerates. Due to lack of expected metal and well-defined

chondrules, low abundances of sulfides, and the presence of vesicles, Al Haggounia 001 suffered a complex classification history. In a first moment was classified as an aubrite; whereas its paired fragments (e.g., NWA 002, 1067, 2736, 2828, 2965, 7401) were classified not only as aubrites but also as different types of enstatite chondrites (EL6, EL6/7, E6, EL3) (e.g., Lowe et al. 2005; Kuehner et al.2006; Irving et al. 2010). Recently, Rubin (2016) reclassified this meteorite as "vesicular, incompletely melted, EL chondrite impact melt rock[s]."

As an EL3 impact melt, this meteorite belongs to enstatite meteorite clan that, among the other groups of meteorites, show to have a highly reduced nature and mineralogy with fO_2 similar to that of Mercury estimated using data from the MErcury Surface, Space ENvironment, GEochemistry, and Ranging (MESSENGER) spacecraft (McCubbin et al. 2012, 2017; Zolotov et al. 2013; Udry et al., 2019). Al Haggounia 001 is characterized by the presence of graphite and sulfides (oldhamite, alabandite and troilite) that represent typical phases found in reduced enstatite chondrite (Szurgot et al., 2011; Rubin 2016). This meteorite exhibits a terrestrial age of about 23,000 +- 2000 yr., as measured by ^{14}C dating (Chennaoui-Aoudjehane et al., 2009) and shows, also, a heavily weathering (W4–W5 grade).

An unusually high porosity characterizes Al Haggounia 001 (Kuehner et al., 2006). This singular feature was previously studied by Rubin (2016) that observed voids in Al Haggounia 001 and its paired meteorite fragments; some were rounded, some irregular and other showed elongated shape. The apparent diameter measured on 40 voids ranged between 50 and 610 μm with an average of around 200 _+ 140 μm. The modal abundance of voids observed by optical observations in transmitted light of NWA 7401 is 6.8 vol% (Rubin, 2016). The same author also found petrographic features consistent with incompletely melted rocks by impact. In fact, he observed vesicles on NWA 7401 paired with Al Haggounia 001 similar to those observed on ordinary-chondrite impact-melt breccias and impact-melt rocks.

The finding of porosity in meteorites and its origin was a long time debated. The first studies were done by Alexayeve (1958), Stacy et al. (1961) and Keil (1962). More recently, Consolmagno et al., (2008) compared meteorite density and porosity and physical properties of their parent bodies and they focused on chondrites belonging to different classes and petrological group. Soini et al. (2020), studied the thermal conductivity, the thermal diffusivity and porosity mainly on the chondrite groups. Lately, the origin of porosity was investigated directly visualizing the volume distribution, density and shape of pores by means of a useful and innovative technique: micro–X-ray Computed Tomography (μCT). This technique has been increasingly used in the meteoritics studies to explore phase distribution, microstructures, crystal habits or grains, occurrences of porosity, melt veins and fractures in a 3D reconstruction of a small meteorite volume, as reported in reviews by Pratesi et al. (2014) and Hanna and Ketcham, (2018). This technique has been mainly applied to the study of texture and distribution of mineral phases, shapes of chondrules and pore distribution on chondrites (Panerai et al., 2021 and references therein); on meteorites of Mars (Nascimento-Dias et al., 2019; Porfido et al., 2020); on enstatite meteorites, (Krzesińska et al., 2019); on stardust impact tracks (Tsuchyama

et al., 2009), silicate inclusions in meteoritic chromite grains (Alwmark et al., 2011), splashform moldavites (Pratesi et al., 2014) and micrometeorites (Dion net et al., 2020).

In the present study, we apply a combined use of μ–CT and chemo-mineralogical analyses by Scansion Electron Microscopy (SEM) to three-dimensionally reconstruct the internal structure, the grain features and porosity of a fragment of Al Haggounia 001. The innovative methodological approach, based on volumetric investigation, permits to add new elements on the origin of porosity and its implications on the evolution history of this meteorite.

2. Materials and Methods

We studied one thin section and a slab section taken from the same fragment of Al Haggounia 001. The thin section and the slab were investigated by Scanning Electron Microscopy (SEM), after graphite and gold-coating, respectively. The gold coating was done to better identify the C-rich phases.

The slab sample was analyzed also by micro–X-ray Computed Tomography (μ-CT) in two regions, named B1 and B2 (Fig. 1).

The SEM microscope used for qualitative, quantitative chemical analyses, and morphological observations is Zeiss LEO EVO50XVP, coupled with an Oxford X-Max (80 mm^2) Silicon Drift Detector (SDD). It has secondary and backscattered electron (BSE) detectors. Chemical analyses were performed using energy dispersive spectrometers (EDS). The SEM operates with an accelerating potential of 15 KV, a probe current of 500 Pa, and a working distance (WD) of 8.5 mm. Aztec software has been used for maps and microanalysis.

Analyses by μ-CT were performed with Bruker Skyscan 1172 high-resolution μX-CT scanner operating at an X-ray Voltage of 100 kV using an Al filter of 0.5 mm (see scanning and reconstruction parameters in Table 1). Bruker's NRecon software was used to reconstruct μX-CT projection images into two-dimensional cross section (slices) by applying the Feldkamp algorithm (Feldkamp et al., 1984). Cross-section parameters are shown in Table 1. μX-CT datasets were analyzed and visualized using Bruker's CTAn and CTvox software.

Table 1. μ–CT scanning parameters

μX-CT scanner Parameters		Reconstruction Parameters	
Pixel Size (μm)	3	Smoothing	4
X-ray Voltage (Kv)	85	Ring Artifact Correction	7
X-ray Current (μA)	118	Beam Hardening Correction (%)	46
Rotation Step (degrees)	0.28	-	
Filter	Al 0.5mm	-	
Frame Averaging	5	-	

Results

3.1. Scanning Electron Microscope analyses

The chemical and mineralogical analyses were carried out on the slab and on thin section of the fragment of Al Haggounia 001, acquiring chemical maps and several spots of microanalyses. Grain features and internal structures were also observed on Back-Scattered Diffraction (BSD) and Secondary Electron (SE) images. The results show that the sample consists of a matrix of enstatite and plagioclase (Fig. 2) with minor phases such as sulfides (daubréelite, oldhamite and troilite), phosphides (scheirbersite), graphite, tiny kamacite grains, survived to the weathering, and N-bearing phase (sinoite). In addition to primary phases, secondary minerals grown in terrestrial environment were found. The most abundant have a composition of jarosite and halite, whereas some kamacite grains exhibit variable degree of oxidation.

Only one relict chondrule was observed on the surface of the slab section (Fig.3). The chondrule consists of a radial pyroxene with enstatite composition, Na plagioclase and silica mesostasis.

SEM-EDS microanalyses reveal that the average composition of pyroxene is $En_{98.4}$ Fs_{0} $Wo_{1.6}$; whereas that of plagioclase is $Ab_{80.23}$ $An_{11.45}$ $Or_{8.32}$, (table 2).

Table 2. SEM-EDS microanalyses (wt%) of silicates

Plagioclase	**Na_2O**	**MgO**	**Al_2O_3**	**SiO_2**	**K_2O**	**CaO**	**TOT**
Wt %	**9.27 ±0.05**	**2.0 ±0.03**	**19.14 ±0.07**	**65.14 ±0.13**	**1.46 ±0.03**	**2.39 ±0.04**	**99.42**
Number of Ions	**7.99**						

Enstatite	**MgO**	**Al_2O_3**	**SiO_2**	**CaO**	**TOT**
Wt %	**39.15 ±0.08**	**0.56 ±0.03**	**59.26 ±0.12**	**0.88 ±0.03**	**99.85**
Number of Ions	**12,00**				

From the textural point of view, the slab is very porous and exhibit many resorption features. Voids observed on SEM SE images can be distinguished in irregular and rounded shapes. In general, irregular shapes characterize the voids between different crystals.

The resorption features observed regard mainly silicates and Cr, Fe, Mn sulfides. Enstatite grains often appear as scalloped crystals (Fig. 4a). Locally the surface of some plagioclase crystals exhibits rounded "micro-craters" (holes) characterized by smooth walls (Fig.4b). Instead, sulfides exhibit rounded etch-piths similar to popped bubbles mainly on the grains of daubréelite composition, whereas schreibersite grains show smooth, sometimes fractured surfaces (Fig. 5).

3.2 μ-Xray Computed Tomography (μ-CT)

The B1 and B2 volumes of the slab of Al Haggounia 001 were investigated by μ–CT (Fig. 6). The images acquired are characterized by different grayscale intensities proportional to the different X-rays absorption of the volume investigated (Agrosì et al., 2019). The not uniformly X-ray absorption is due to the presence of minerals with different X-ray attenuation coefficients and an uneven distribution of voids. In Figure 6, the phases with highest attenuation coefficient appear white, whereas phases with low to middle attenuation coefficient appear light to medium and dark gray. The attenuation coefficient corresponding to voids is near zero; consequently, the voids appear black. The cross-section images, taken along the B1 and B2 regions, show a variable distribution of phases, an uneven distribution of porosity, and a strong correlation of the spatial distribution of pores (black) with high-density phases (white) (Fig. 6b).

Specifically, the high-density phases (white) are mainly confined near the pores and, in some cases, fill them (Fig. 6). Furthermore, the high-density phases appear most abundant in the outer part of B2 volume. The 3D analysis also allows distinguishing between open and closed pores. Open pores are empty spaces within the meteorite volume that show any connection in 3D to the space outside the object. Closed pores consist of empty spaces in the meteorite volume that are surrounded by solid phases.

To quantify the main components that characterize Al Haggounia 001 slab, five categories were considered selecting thresholds based on peak analyses of the grayscale histogram (0-255) of the rendered volumes.

These categories were assigned as follows:

white: range 181-255 of histogram assigned to highest density phases;

light grey: range 131-180 assigned to the moderately dense phases;

medium grey: 100-130 assigned to moderately less dense phases;

dark grey: 30-99 assigned to the less dense phases in the slab.

Values of histogram <30 were assigned to pores and materials trapped in them, such as air and low-density epoxy resin used for rock embedding.

The 3D results found on the B1 and B2 volumes show significant differences (Tables 3 and 4).

The total porosity of volume B1 results higher than that of volume B2, significantly decreasing in the upper part of B2, where the maximum percentage of closed pores was observed. The average size of open pores is about 0.42 mm both for B1 and B2 volumes; whereas the average size of closed pores is higher in the B2 outer volume (0.035mm) than that of closed pores in the B1 and B2 inner volume (0.025 mm) (Tab. 3 and Fig. 7).

Table 4 reports the percentage of the other four solid categories (181-255, 131-180, 100-130 and 30-99 ranges of histogram values). Their percentages were calculated considering only the volume of solid phases, excluding the porosity volume. The volume percentage of phases with high-density (histogram values between 100-255) is significantly higher in the outer part of the B2 volume (about 4%) than B1 volume and the inner part of volume B2 (about 0.170%), confirming what observed qualitatively in Fig. 6a.

Table 3. Volume percentage and sizes of pores measured on volumes B1 and B2 and the outer and inner parts of B2.

	Thresholds on grey-scale histo-gram	B1	B2	B2inner	B2outer
Total porosity (vol. %)	≤30	17.52	13.08	14.31	9.27
Open pores (vol. %)	≤30	15.00	9.47	11.51	5.13
Closed pores (vol. %)	≤30	2.52	3.61	2.80	4.14
Solid phases (vol %)	31-255	82.48	86.92	85.69	90.73
Average size of open pores (mm)	≤30	0.041	0.043	0.043	0.041
Average size of closed pores (mm)	≤30	0.024	0.030	0.026	0.035

Table 4. Volume percentage of the main threshold ranges, calculated considering only the solid phases, measured on volumes B1 and B2 and the outer and inner parts of B2.

Gray level	Thresholds on grey-scale histo-gram	B1	B2	B2 inner	B2 outer
White (%)	181-255	0.019	0.062	0.020	0.152
light grey (%)	131-180	0.053	0.519	0.052	1.551
medium grey (%)	100-130	0.095	0.805	0.100	2.361
dark grey (%)	31-99	99.835	98.598	99.825	95.975

3.3 Merging of SEM-EDS and μ-CT data

To quantify approximately the spatial distribution and the volume percentage of mineralogical phases, we merge SEM-EDS microanalyses with the results of the volume rendering segmentation of μ-CT data. The threshold ranges on grey scale histogram were assigned to the corresponding minerals considering the Linear Attenuation Coefficient (LAC) values of the main phases identified with SEM-EDS analyses. LAC was also calculated for iron oxide and hydroxides formed by the oxidation of kamacite. Minerals with similar LAC were grouped, and for each group the correspondence with the grayscale color of thresholding is listed in Table 5.

Table 5. Minerals with similar LAC grouping under same grayscale color. LAC calculated by MuCalc software (Hanna and Ketcham, 2017) and MXLAC software (Bam et al., 2020)

Mineralogical phases	formula	LAC (Energy =60 keV)	Color categories	Thresholds on grayscale histogram
kamacite	(Fe,Ni)	9.444	white	181-255
schreibersite	$(Fe,Ni)_3P$	7.750		
wustite	$Fe^{2+}O$	5.4	light gray	131-180
hematite	$Fe^{3+}{}_2O_3$	4.729		
troilite	$Fe^{2+}S$	4.210		
goethite	$Fe^{3+}O(OH)$	3.57		
daubreelite	$Fe^{2+}Cr_2S$	2.880	medium gray	100-130
jarosite	$KFe^{3+}{}_3(SO_4)_2(OH)_6$	1.760		
oldhamite	$Ca_{0.9}Mg_{0.05}Fe^{2+}{}_{0.05}S$	1.370		
enstatite	$Mg_2Si_2O_6$	0.871	dark gray	31-99
halite	NaCl	0.771		
sinoite	Si_2N_2O	0.740		
Silica mesostasis	SiO_2	0.666		
albite	$Na_{0.95}Ca_{0.05}Al_{1.05}Si_{2.95}O_8$	0.642		
graphite	C	0.390		

The data comparison shows that the dark grey phases (33-99 thresholding) consist mainly of silicates (enstatite and plagioclase) with other less abundant phases such as sinoite, graphite and secondary halite. Sulfides and secondary phases such as jarosite, iron oxides and hydroxides represent the intermediate gray scale up to white corresponding to schreibersite and kamacite. The inhomogeneous spatial distribution of phases and pores in the B1 and B2 volumes of slab, their volume percentages, and the different pores sizes are shown in table 6 and Figure 7.

Table. 6 volume percentage of the five categories of thresholds based on peak analyses of the grayscale histogram (0-255) of the whole rendered volumes

phases	thresholding	Vol. % B1	Vol. %B2 inner	Vol. % B2 outer
kamacite	181-255	0.012	0.017	0.138
schreibersite				
wustite	131-180	0.028	0.044	1.411
hematite				
troilite				
goethite				
daubreelite	100-130	0.048	0.085	2.147
jarosite				
oldhamite				
enstatite	31-99	82.392	85.544	87,035
halite				
sinoite				
Silica mesostasis				
albite				
graphite				
Total porosity	≤ 30	17.52	14.31	9.269
Closed pores		2.52	3.17	4.139

The volume percentage of silicates is very high and represents on average 84.00% of the total volume. The moderately and moderately less dense phases, consisting of iron oxides and hydroxides, troilite, daubréelite, jarosite and oldhamite, represent low amounts with significant difference between B1 and B2 region and the outer part of B2 region. The amount of schreibersite and kamacite is very low under the spatial resolution of μ-CT. Grains with size less than 3 μm could be present, but not considered in this calculation.

4. Discussion

The obtained results show that the studied fragment is not homogeneous regarding the spatial distribution of porosity and high-density phases. The porosity has been measured on a volume of sample, distinguishing, for the first time, between open and closed pores. The average total porosity is almost consistent with a previous study performed by Abassi et al., 2013 who found in Al Haggounia 001 meteorite a porosity of 12.4 ± 1.2 %, using ultrasonic reflectivity method with a spatial resolution of 0.7 μm and considering only open pores. The average porosity calculated B1 and B2 is about 12.20% of volume, considering only the open pores. Since the heterogenous texture of Al Haggounia 001 and its paired samples and the different principles of the used techniques with a slightly different spatial resolution, the volume percentage of open pores, in both cases measured on a volume of meteorite, fit very well. Nevertheless, the value of total porosity, also considering the closed pores, increases significantly. The distribution of closed pores is very different in the studied slab and shows lower concentration in volume B1 and higher value in the volume B2, particularly in its outer part. This inhomogeneity can be related to the spatial distribution of the high-density phases. The combined analyses on the B1 and B2 volumes of the slab, merging μ-CT data and SEM-EDS, allow us to associate the decrease of total porosity with the increase of the volume percentages of both the high-density phases and the closed pores in the outer part of the B2 region, suggesting that secondary phases, such as jarosite and iron oxides and hydroxides, fill up in part the porosity, reducing it and favoring the formation of closed pores. This phenomenon seems to interest mainly the fragment region more exposed to terrestrial weathering. However, the origin of porosity needs to be better explained. The porosity in meteorites is generally related to terrestrial weathering processes of, even if the origin of porosity in chondrites is a still debated topic (Irving et al., 2010; Li et al., 2019). The high porosity of Al Haggounia can be interpreted also considering the grain features, the mineralogical composition and relationships between voids and solid phases of this meteorite. The studied fragment shows a very low content of high-density phases, excluding

the silicates. The phases corresponding to 100-255 of thresholding in the 3D volume rendering, show a volume percentage of 0.088% in region B1, 0.146% in the inner part of volume B2 and a higher value of 3.696% in the outer part of volume B2. If we consider that the increase of high-density phases in the outer part of B2 is due to a high quantity of secondary phases (Jarosite and iron oxides and hydroxides), sulfides, kamacite and schreibersite represent a very little amount. Furthermore, among the sulfides found in this study, troilite represents a very tiny amount. This finding contrasts with the composition of EL3 chondrites that generally contain about 10 vol% of sulfides with a prevalent presence of troilite (about 90 vol%) (Weisberg and Kimura 2012; El Goresy et al., 2017). The smaller grains of 3 μm could not be found because of the spatial resolution of μ-CT analyses, but this resolution-limit is insufficient to explain the little amount of troilite.

The low content of high-density phases could be ascribed not only to the severe weathering but also to degassing of sulfides during melting by impact event that may have contributed to developing the vesicles and porosity. This latter process is supported by the presence of resorption features observed on enstatite crystals, microcraters on plagioclases and etch pits like bubbles on Cr-rich sulfides, which represent further proves of incompletely melting by shock events, as previously stated by Rubin (2016). On the other hand, excluding the precipitation of secondary phases that interests locally the voids (outer part of volume B2), the B1 and the inner part of B2 regions show a uniform pore distribution (Fig. 7). One possible explanation could be that part of voids were initially occupied by high-density phases homogeneously spread in the sample. The uniform distribution of these hypothetical primary phases and their successive disappearance that left the voids, would indicate a triggering phenomenon acting not only locally, but on the entire meteorite body such as an impact and/or high-grade metamorphism. These phases could be just sulfides and, in particular, troilite, now almost not present. This supposition confirms previous hypotheses stated by Lauretta (1997), Rubin (2016) and Panerai et al., (2021). In particular, Panerai et al. (2021) found strong relationships between sulfide degassing of and origin of porosity, analyzing by μ–CT two ordinary chondrites undergoing a range of temperatures from ambient to 1200 C°.

Our results, therefore, suggest that the high porosity found in Al Haggounia 001 fragment could be due to different events: during melting by impact event the degassing and evaporating of sulfides left voids and vesicles and produced resorption features by partial melting also on silicates, preserving some relict chondrules; successively, after the fall of meteorite, severe weathering in part enlarged the previous pores and vesicles and in part fill up locally some of them by the precipitation of terrestrial phases.

Conclusions

The volumetric data acquired on the internal structure and grain features of Al Haggounia 001 add new elements to this heterogeneous meteorite. A new estimation of total porosity for Al Haggounia 001, the differentiation between open and closed pores and the interpretation of the relationships between the spatial distribution of voids and the different mineralogical phases suggest different genetic processes of voids formation. The resorption features and the almost homogeneous distribution of open pores heavily support the previous hypothesis of Rubin (2016) who assigned the formation of voids and vesicles to degassing and evaporating of sulfides (mainly troilite) during melting by impact events. Conversely, the presence of closed pores can be ascribed to the terrestrial weathering, that locally operated on exposed pores, determining a partial filling by precipitation of secondary phases.

With this work we show the importance of a methodological approach that investigate a volume of a fragment of meteorite, providing a reconstruction of the spatial distribution of mineralogical phases and voids, their volume percentage, shape, and size. The volumetric analyses reduce the error generally related to data acquired on nearly bidimensional sample such as a thin section, minimizing the risk to obtain dissimilar information on different fragments of the same meteorite.

References

1. Agrosì G., Tempesta G., Mele D., Caggiani M.C., Mangone A., Della Ventura G., Cestelli-Guidi M., Allegretta I., Hutchison M. T.; Nimis P., Nestola, F., 2019. Multiphase inclusions associated with residual carbonate in a transition zone diamond from Juina (Brazil). Lithos, 350-351, http://www.journals.elsevier.com/lithos/ doi: 10.1016/j.lithos.2019.105279
2. Alexayeve, K.N., 1958. Physical properties of stony meteorites and their interpretation based on the hypothesis on the origin of meteorites. Meteoritika 16, 67–77.
3. Alwmark, C., Schmitz, B., Holm, S., Marone, F. and Stampanoni, M., 2011. A 3-D study of mineral inclusions in chromite from ordinary chondrites using synchrotron radiation X-ray tomographic microscopy—Method and applications. Meteoritics & Planetary Science 46, 1071-1081. https://doi.org/10.1111/j.1945-5100.2011.01214.x.
4. Bam L.C., Miller, J.A., Becker, M. 2020**.** A Mineral X-ray Linear Attenuation Coefficient Tool (MXLAC) to Assess Mineralogical Differentiation for X-ray Computed Tomography Scanning. Minerals, 10, 441. https://doi.org/10.3390/min10050441
5. Bunch T, Wittke J., Irving A.J., 2014. http://www4.nau.edu/meteorite/Meteorite/Al_Haggounia.html
6. Chennaoui-Aoudjehane H., Jambon A., and Rjimati E. 2007. Al Haggounia (Morocco) strewn field. Meteoritics & Planetary Science 42, A30.
7. Consolmagno G., Britt D. and Macke R., 2008. The significance of meteorite density and porosity. Chemie der Erd Geochemistry 68(1),1–29. doi: 10.1016/j.chemer.2008.01.003.
8. Dionnet Z., Suttle M.D., Longobardo A., Rotundi A., Folco L., Della Corte V. and King A., 2020. X-ray computed tomography: Morphological and porosity characterization of giant Antarctic micrometeorites. Meteorit. Planet Sci. 55, 1581-1599. https://doi.org/10.1111/maps.13533
9. El Abassi, D., Ibhi, A., Faiz, B., Aboudaoud, I. 2013. A simple method for the determination of the porosity and tortuosity of meteorites with ultrasound. Journal of Geophysics and Engineering 10(5), https://doi.org/10.1088/1742-2132/10/5/055003.
10. El Goresy A., Lin Y., Miyahara M., Gannoun A., Boyet M., Ohtani E., Gillet P., Trieloff M., Simionovici A., Feng L., And Lemelle L., 2017. Origin of EL3 chondrites: Evidence for variable C/O

ratios during their course of formation—A state of the art scrutiny. Meteoritics & Planetary Science 52(5), 781–806 doi: 10.1111/maps.12832781©The Meteoritical Society, 2017.
11. Hanna and Ketcham, 2017. https://www.ctlab.geo.utexas.edu/software/mucalctool/ Romy D. Hanna, Richard A. Ketcham, X-ray computed tomography of planetary materials: A primer and review of recent studies, Geochemistry, Volume 77(4), 547-572, ISSN 0009-2819. https://doi.org/10.1016/j.chemer.2017.01.006.
12. Irving A. J., Bunch T. E., Rubin A. E., and Wasson, J. T., 2010. Northwest Africa 2828/Al Haggounia 001 is a Weathered, Unequilibrated EL Chondrite: Trace Element and Petrologic Evidence, Meteoritics and Planetary Science Supplement, vol. 73.
13. Keil, K., 1962. Quantitativ-erzmikroskopische Integrationsanalyse der Chondrite. Chem. Erde 22, 281–348.
14. Krzesińska, A.M., Wirth R. and Kusiak M.A., 2019. Petrogenesis of ungrouped enstatite meteorite Zakłodzie: Fabric, texture, and nanostructure analysis for identification of mechanisms responsible for chondrite–achondrite transition. Meteorit Planet Sci 54, 1462-1477. https://doi.org/10.1111/maps.13296
15. Kuehner S. M., Irving A. J., Bunch T. E., and Wittke, J. H.0., 2006. EL3 Chondrite (not Aubrite) Northwest Africa 2828: An Unusual Paleo-meteorite Occurring as Cobbles in a Terrestrial Conglomerate. (abstract #P51E-1247). American Geophysical Union, Fall Meeting 2006
16. Lauretta DS, Lodders K, Fegley B. Experimental simulations of sulfide formation in the solar nebula. Science (New York, N.Y.). 277, 358-60. PMID 9219690 DOI: 10.1126/Science.277.5324.358
17. Li S. J., Wang S. J., Miao B. K., Li Y., Li X. Y., Zeng X. J., & Xia, Z. P., 2019. The density, porosity, and pore morphology of fall and find ordinary chondrites. Journal of Geophysical Research: Planets, 124, 2945– 2969. https://doi.org/10.1029/2019JE005940.
18. Lowe J.J., Hill D.H., Domanik, K.J. Lauretta, D.S., Drake M.J., Killgore M., 2005. NWA 2736: An Unusual New Graphite-bearing Aubrite. 36th Annual Lunar and Planetary Science Conference.
19. McCubbin F. M., 2017. A Low O/Si Ratio on the Surface of Mercury: Evidence for Silicon Smelting? Journal of Geophysical Research (Planets), 122 (10), 2053–2076. doi:10.1002/2017JE005367.
20. McCubbin, F. M., Riner, M. A., Vander Kaaden, K. E., and Burkemper, L. K., 2012. Is Mercury a volatile-rich planet?. Geophysical Research Letters 39(9) doi:10.1029/2012GL051711.
21. Nascimento-Dias BL, Araujo OMO, Machado AS, Oliveira DF, Anjos MJ, Lopes RT, Assis JT., 2019. Analysis of two meteorite fragments (lunar and martian) using X-Ray micro fluorescence and X-Ray computed microtomography techniques. Appl Radiat Isot. 152, 156-161. doi: 10.1016/j.apradiso.2019.06.021. Epub 2019 Jun 19. PMID: 31302533.
22. Panerai F., Bessire B., Haskins J., Foster C., Barnard H., Stern E., Feldman J., 2021. Morphological Evolution of Ordinary Chondrite Microstructure during Heating: Implications for Atmospheric Entry. The Planetary Science Journal 2. doi:10.3847/PSJ/ac1749
23. Porfido, C., Manzari, P., Allegretta, I., Terzano, R., De Pascale, O., & Senesi, G.S. 2020. Combined micro-X-ray fluorescence and micro computed tomography for the study of extraterrestrial volcanic rocks. The case of Northwest Africa (NWA) 8657: A shergottite martian meteorite. Talanta 217, 121114.
24. Pratesi G, Caporali S, Loglio F, Giuli G, Dziková L, Skála R. 2014. Quantitative Study of Porosity and Pore Features in Moldavites by Means of X-ray Micro-CT. Materials (Basel). 24;7(4):3319-3336. doi: 10.3390/ma7043319. PMID: 28788620; PMCID: PMC5453340.
25. Rubin, A. E., 2016. Impact melting of the largest known enstatite meteorite: Al Haggounia 001, a fossil EL chondrite. Meteoritics and Planetary Science. 51(9) 1576–1587, 2016. doi:10.1111/maps.12679.
26. Soini A.-J., Kukkonen I.T., Kohout T. and Luttinen, A., 2020. Thermal and porosity properties of meteorites: A compilation of published data and new measurements. Meteorit Planet Sci, 55, 402-425. doi.org/10.1111/maps.13441
27. Stacy F.D., Lovering J.F., Parry L.G., 1961. Thermomagnetic properties, natural magnetic moments, and magnetic anisotropies of some chondritic meteorites. J. Geophys. Res. 66, 1523–1534.
28. Szurgot M., Polanski K., and Kosinski J. W. 2011. Microscopic studies of Al Haggounia 001 meteorite. Scientific Bulletin of the Technical University of Lodz, Physics 32, 65–74.

29. Udry A., Wilbur, Z. E., McCubbin, F. M., Vander Kaaden K. E., Ziegler K. G., De Felice C., McCoy T., Gross J., Turrin B. D., 2019. Aubrite meteorites as geochemical analogues to Mercury. https://ui.adsabs.harvard.edu/abs/2019AGUFM.P11B..01U.
30. Weisberg M. K. and Kimura M. 2012. The unequilibrated enstatite chondrites. Chemie der Erde 72,101–115.
31. Zolotov M.Y., Sprague A.L., Hauck S.A., Nittler L.R., Solomon, S.C., Weider S.Z. 2013. The redox state, FeO content, and origin of sulfur-rich magmas on Mercury. Journal of Geophysical Research (Planets) 118, 138–146. doi:10.1029/2012JE004274.

Figure captions

Figure 1. Optical image of the of Al Haggounia meteorite fragment. The red rectangles, named B1 and B2, represent the volumes analyzed by micro-X-ray-Computed Tomography (μ-CT).

Figure 2. a) SEM-BSD image of Al Haggounia 001 thin section. b) Elemental maps overlayed on BSD image. blue= enstatite; yellow=plagioclase.

Figure 3. Radial pyroxene chondrule in the sample of Al Haggounia 001 a) SEM-BSD image; b) Mg elemental map.

Figure 4. Images of resorption features on Al Haggounia 001 a) SEM-BSD image of scalloped enstatite and corresponding EDS spectrum; b) SEM-SE images of sub-spherical and rounded holes on Na-plagioclase and corresponding EDS spectrum.

Figure 5. SEM images and corresponding EDS spectra. a) SEM-BSD image of daubréelite grain showing round circular etch pits b) SEM-SE image of daubréelite grain showing round circular etch pits c) SEM-BSD image of fractured schreibersite grain.

Figure 6. μ-CT images of Al Haggounia 001 slab. Black=pores. Grey to white=phases with increasing X-ray attenuation coefficient. a) Volume rendering images of B1 and B2 regions. Red line divides the outer part (right) from the inner part (left) of B2 volume. b) cross-section images taken along the blue and red lines of B1 and B2 volumes.

Figure 7. Pore size distribution histograms of the B1 region and inner and outer parts of the B2 region.

Figure 8. B1 region of Al Haggounia 001 slab. a) SEM-BSD image; b) 3D volume rendering with phases corresponding to 100-255 of thresholds on grayscale histogram. Note the random distribution of the high-density phases.

Figure 9. B2 region of Al Haggounia 001 slab. a) SEM-BSD image; b) 3D volume rendering with phases corresponding to 100-255 of thresholds on grayscale histogram and open (blue) and closed pores (yellow); c) 3D volume rendering with only the high-density phases (100-255 of thresholds on grayscale histogram). d) SEM-EDS elemental map of S; e) SEM-EDS elemental map of K; SEM-EDS elemental map of Fe. Note the increase of high-density phases in the outer part, corresponding to the presence of Fe-rich phases and Jarosite (see K elemental map).

Figure 1

Click here to download Figure figure 1.pdf

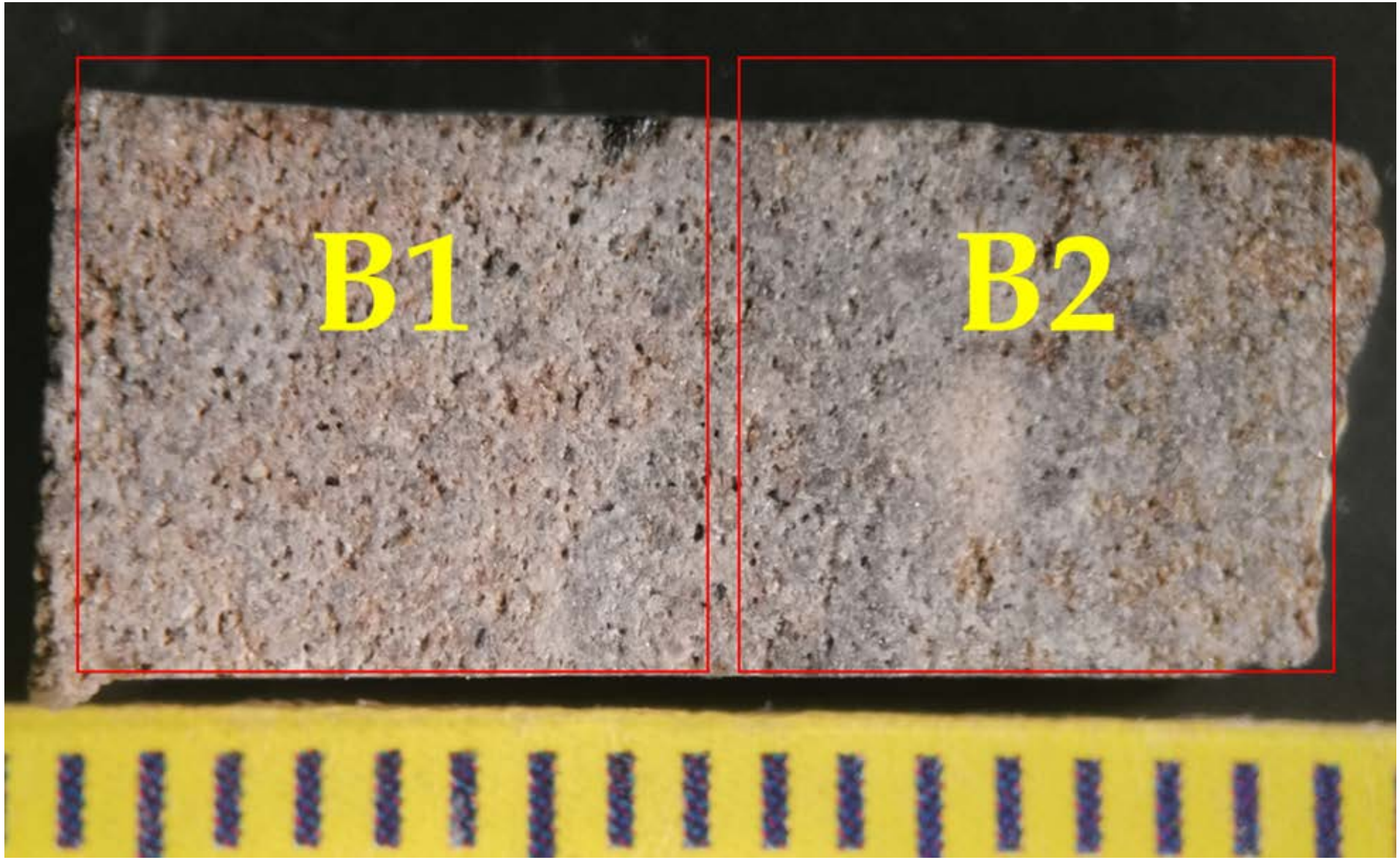

Figure 2

Click here to download Figure figure 2.pdf

a)

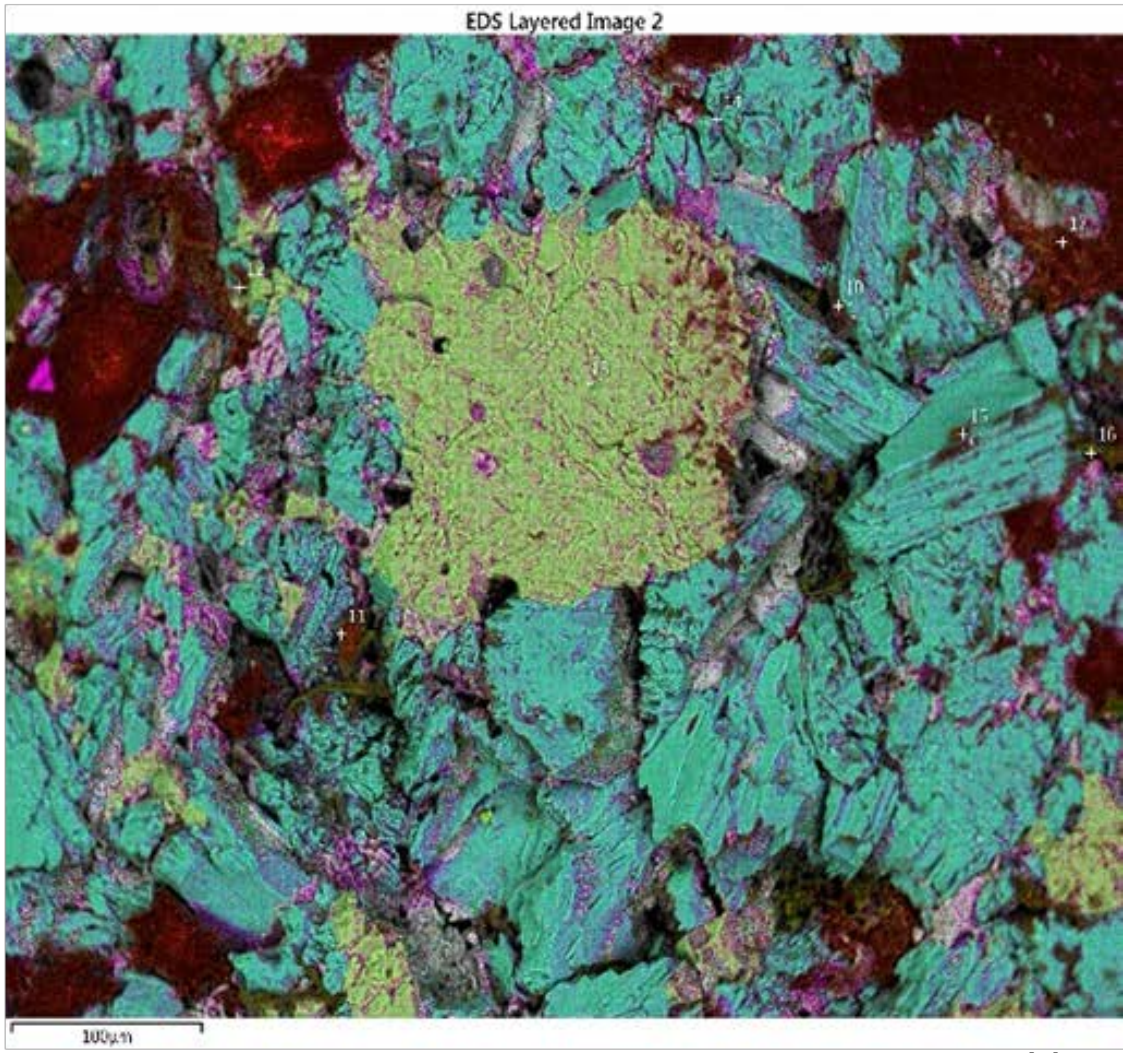

b)

Figure 3

Click here to download Figure figure 3.pdf

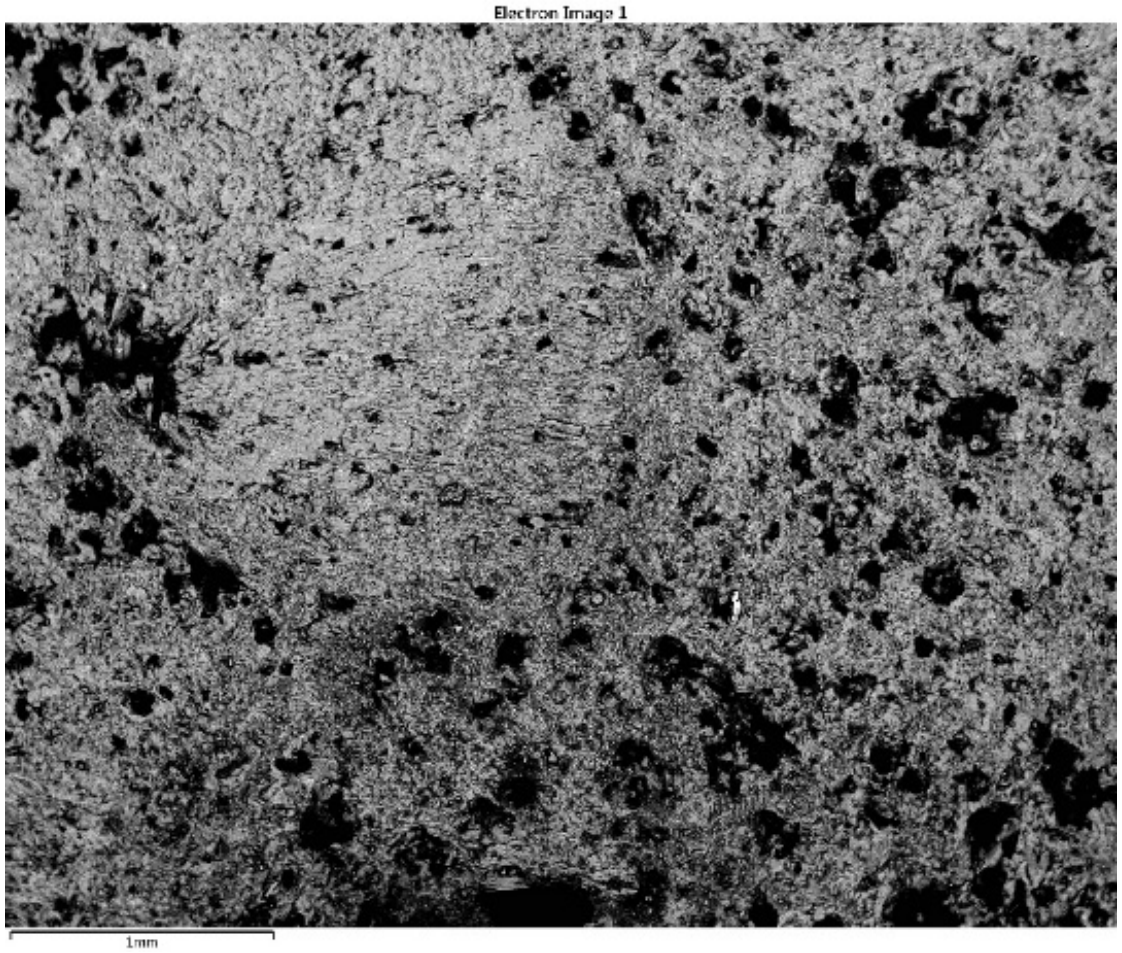

a)

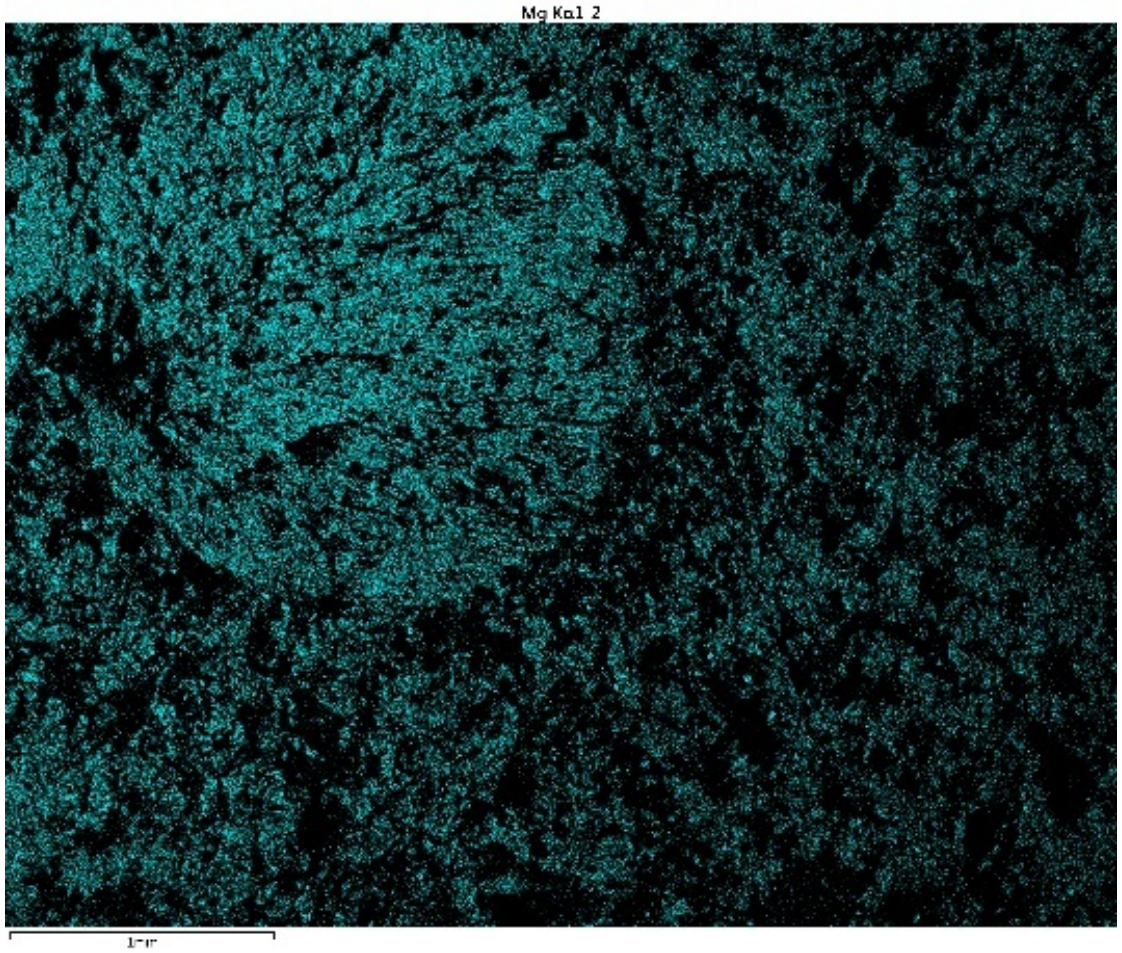

b)

Figure 4

Click here to download Figure figure 4.pdf

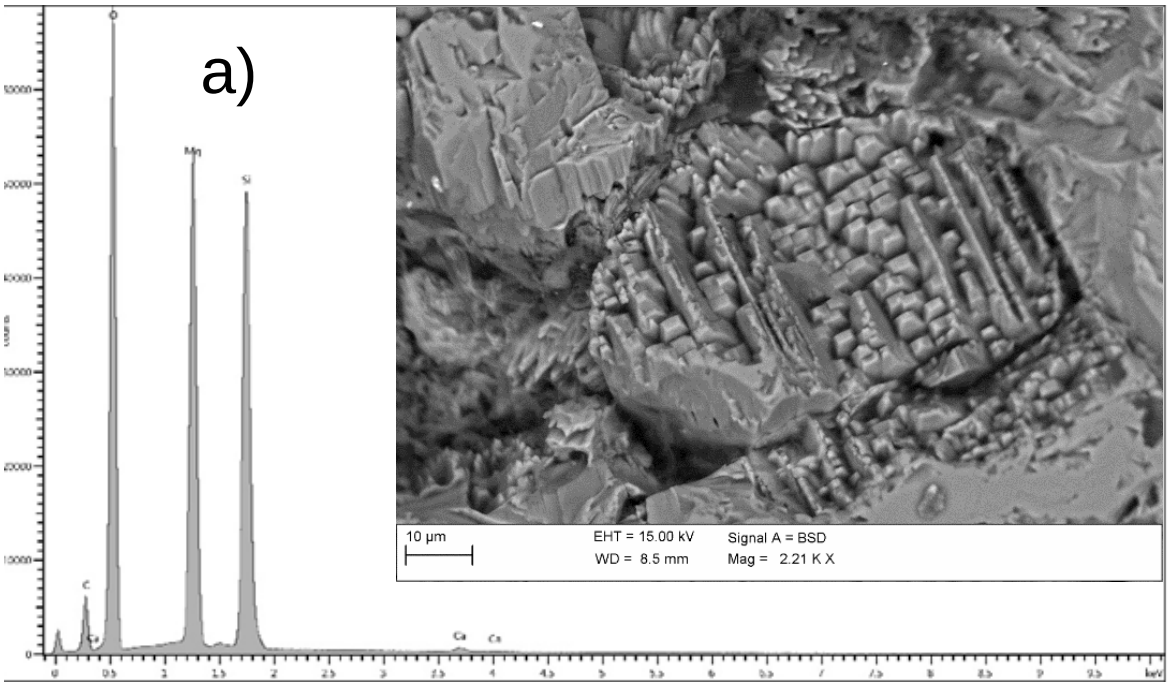

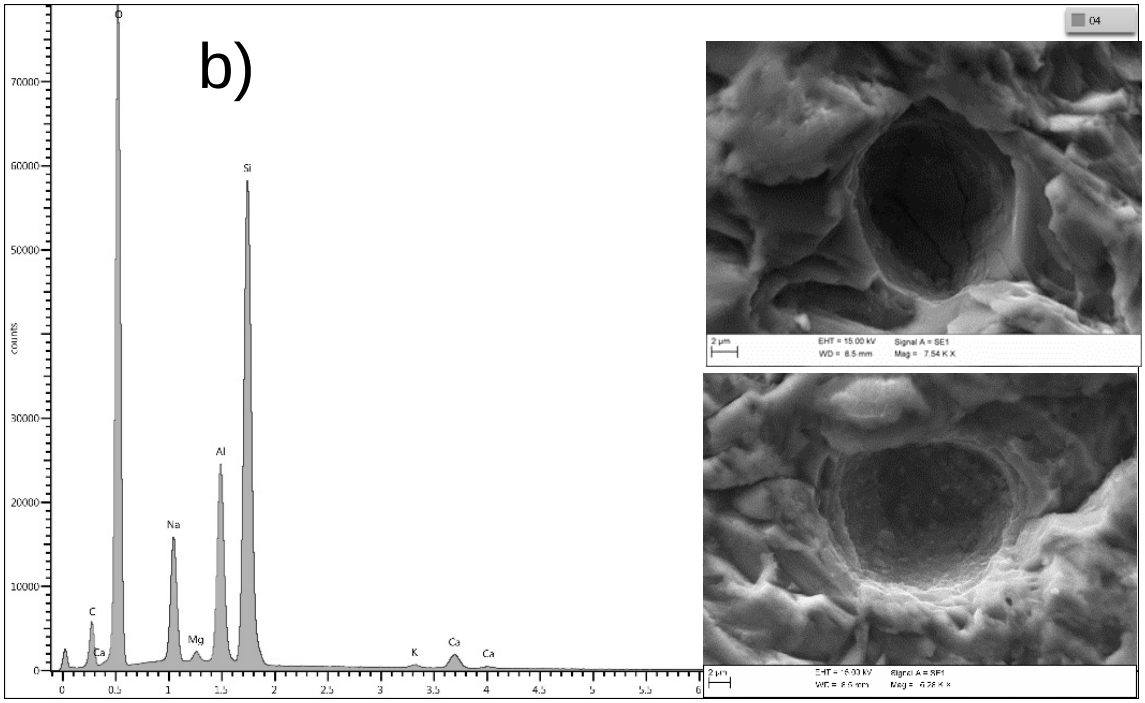

Figure 5

Click here to download Figure figure 5.pdf

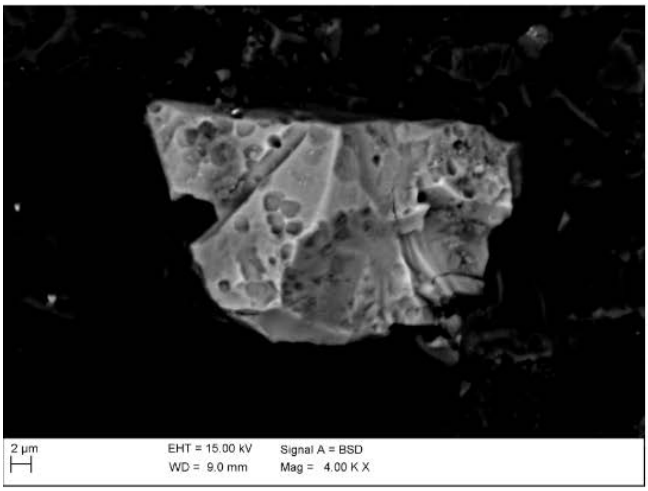

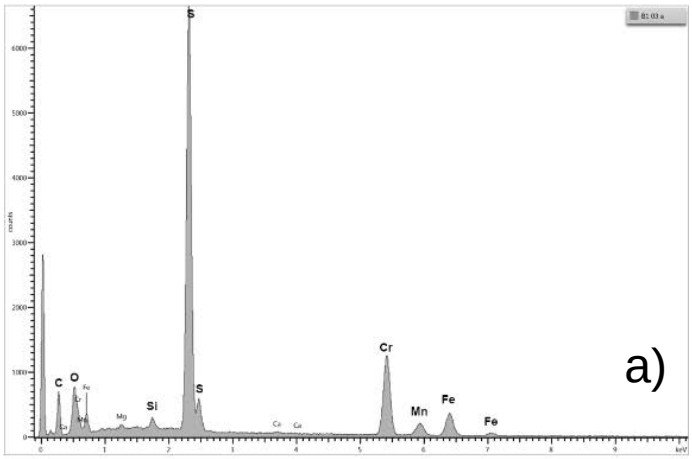

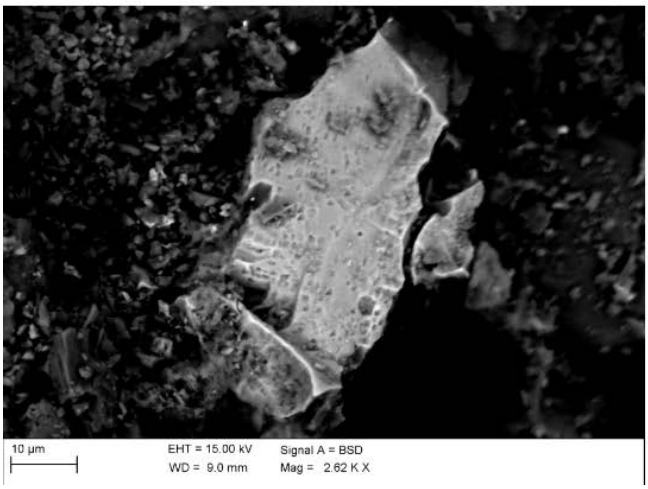

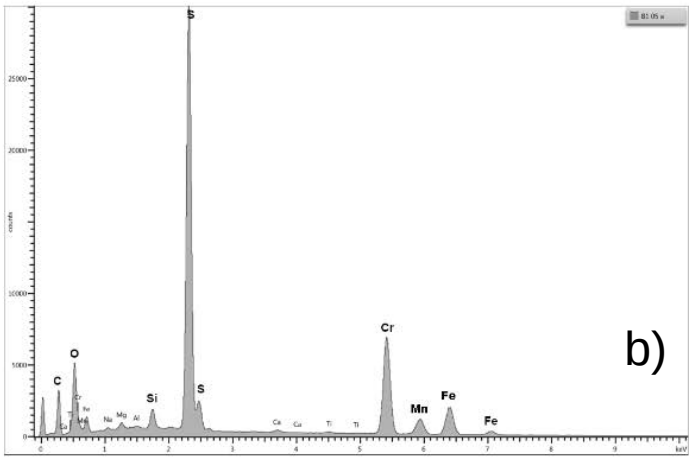

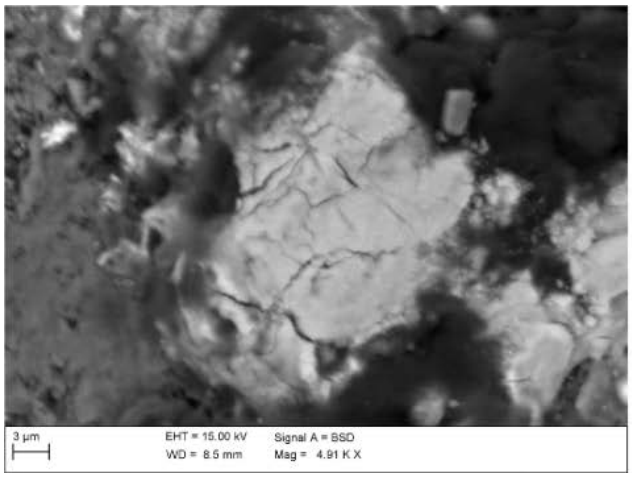

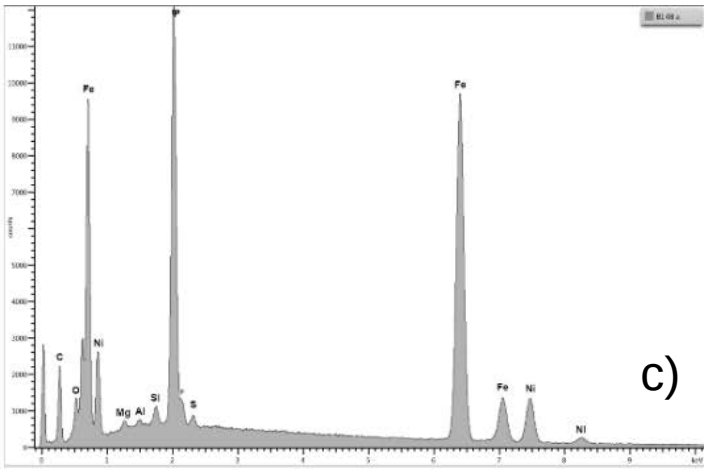

Figure 6

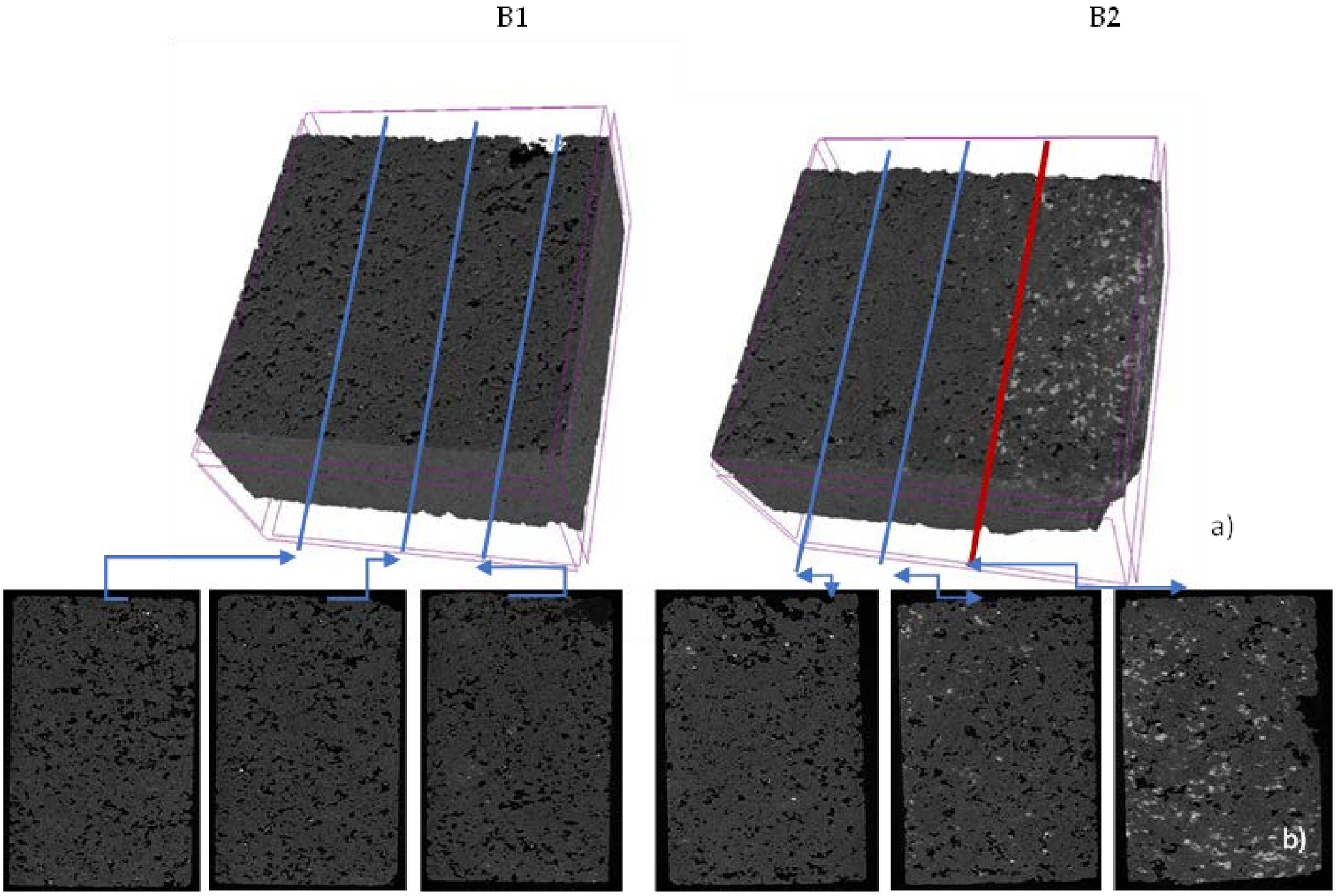

Figure 7

Click here to download Figure figure 7.pdf

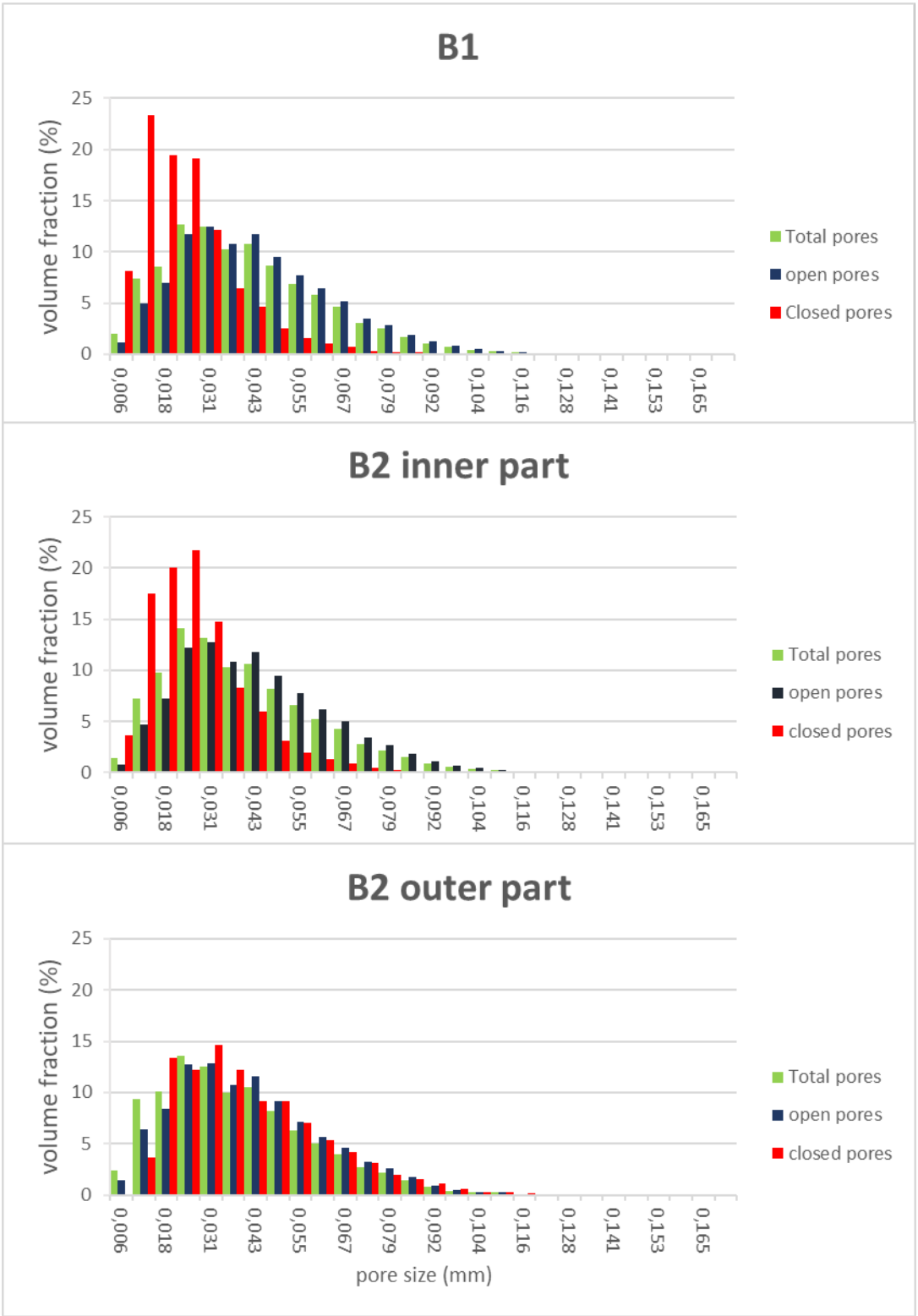

Figure 8

Click here to download Figure figure 8.pdf

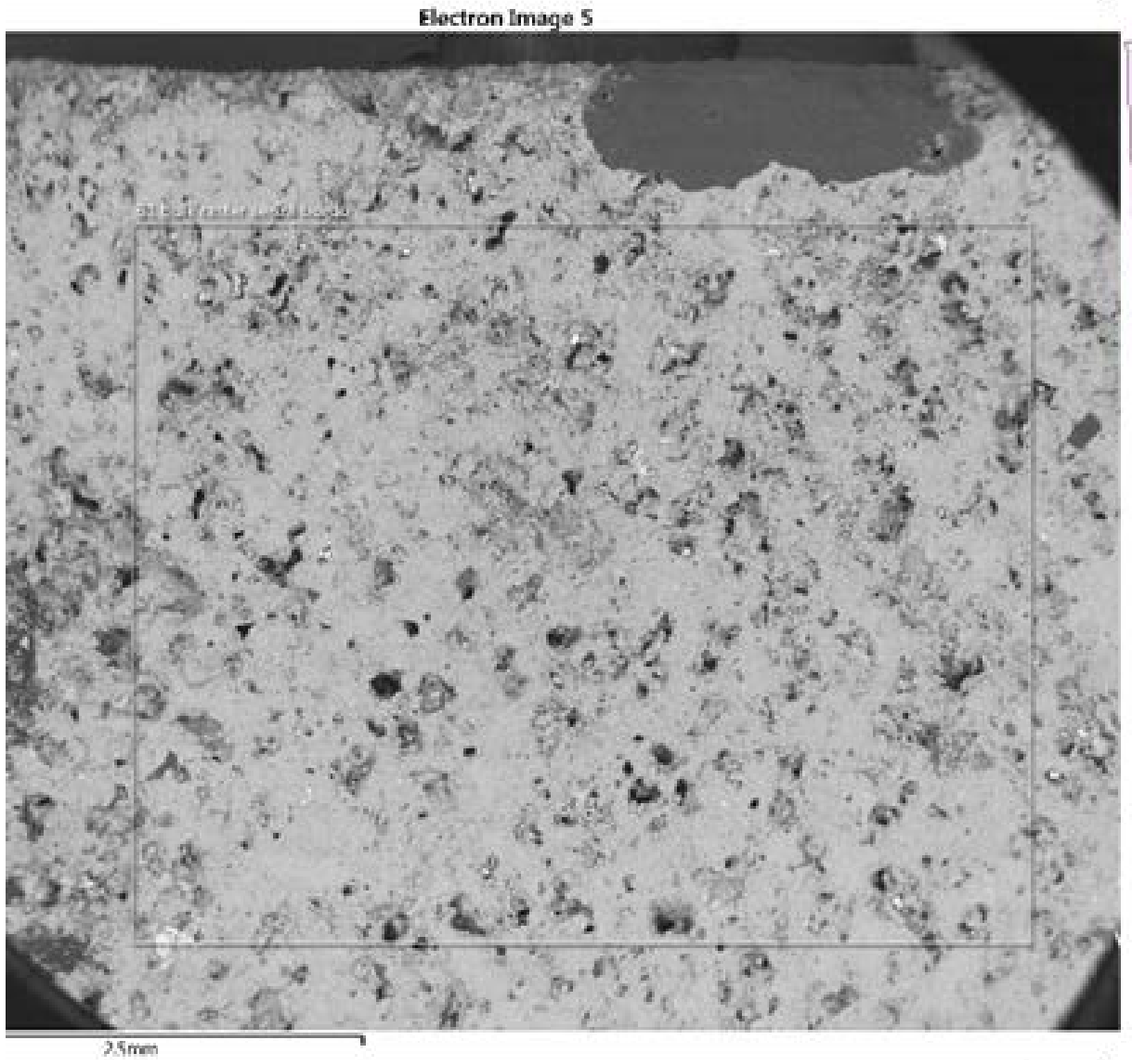

a)

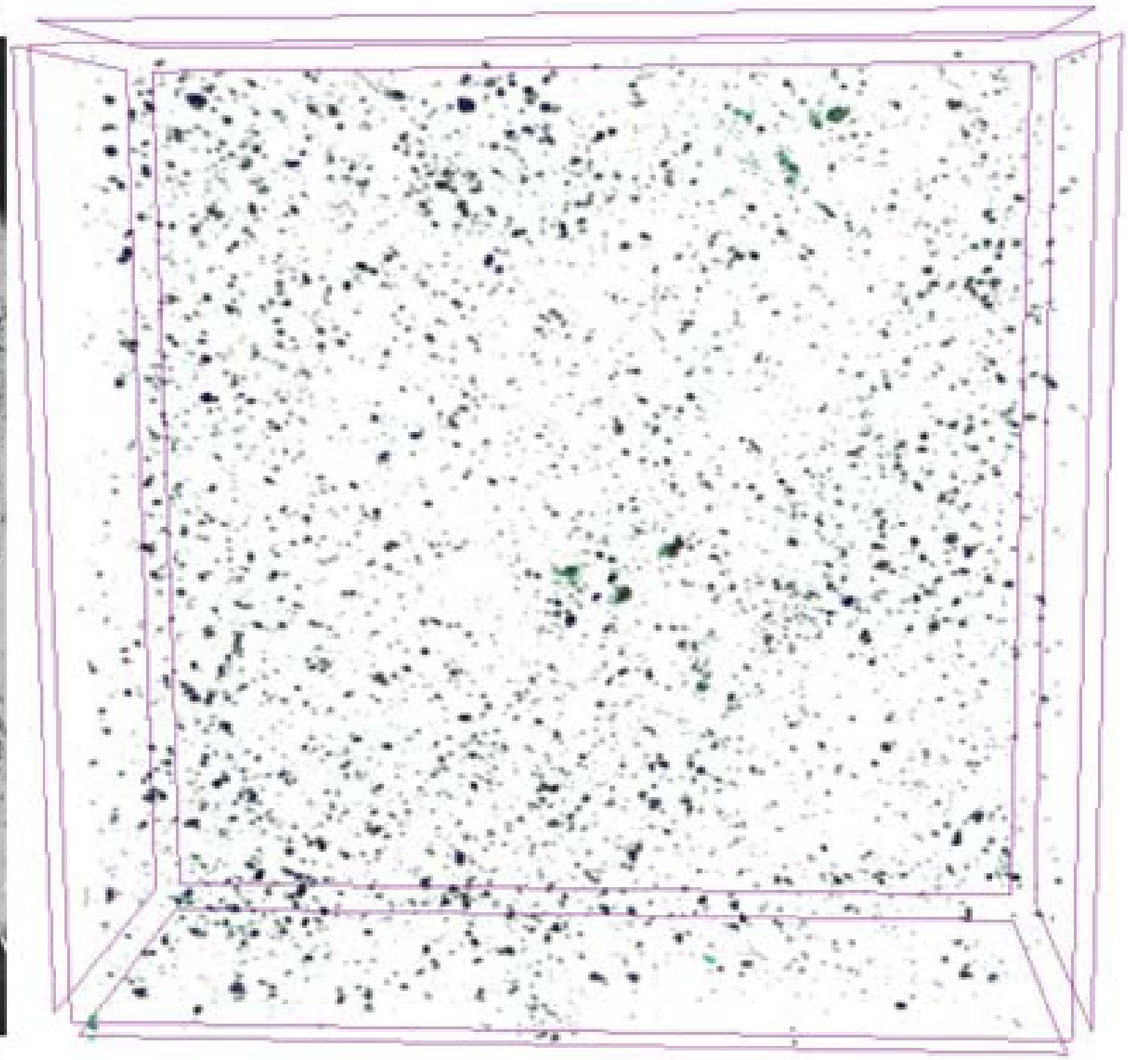

b)

Figure 9

Click here to download Figure figure 9.pdf

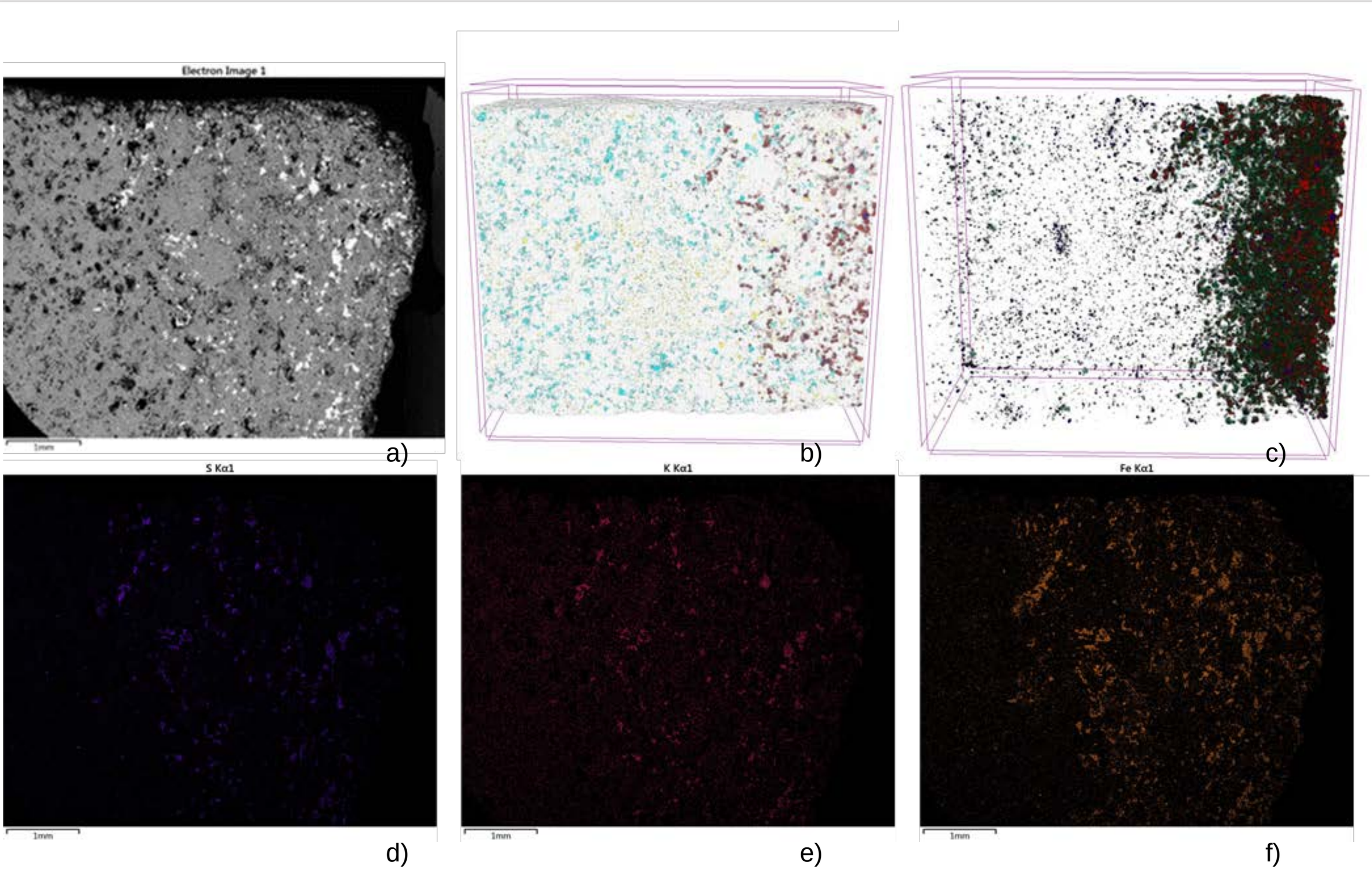

Declaration of interests

☒The authors declare that they have no known competing financial interests or personal relationships that could have appeared to influence the work reported in this paper.

☐The authors declare the following financial interests/personal relationships which may be considered as potential competing interests: